Aeroacoustic Study of Lift Offset Coaxial Rotor using Free Wake Analysis

Kalki Sharma Ph.D. Candidate
Kenneth S. Brentner Professor
Penn State University
University Park, PA, USA

Zhongqi Jia Ph.D. Candidate
Seongkyu Lee Assistant Professor
University of California, Davis
Davis, CA, USA

ABSTRACT

This paper performs aerodynamic and acoustic analysis on a coaxial rotor system based on the XH-59A coaxial helicopter. The aerodynamic analysis is performed in RCAS using free wake modeling, and the acoustic prediction is performed with PSU-WOPWOP, which utilizes Farassat's Formualation 1A of the Ffowcs Williams-Hawkings equation. The coaxial rotor system is analyzed for forward flight speeds of 100 knots and 150 knots. For each case the rotor shaft angle and the distribution of loading is varied to understand the impact on the rotor noise and the aerodynamic environment of the rotor system. The aerodynamic environment is analyzed by wake and blade load visualization, and the noise is computed on a hemi-spherical grid 10 rotor radii from the coaxial rotor system.

INTRODUCTION

A coaxial helicopter is a rotorcraft configuration which relies on two coaxial, contra-rotating rotors for its primary flight capabilities. The rotors contra-rotate on a single axis with a separation distance between the two rotors dependent primarily on the blade deflection. Many modern coaxial configurations also rely on additional vehicle components to augment the lift and/or thrust of the rotors – these vehicles are referred to as compound rotorcraft. Over the years, companies have researched and developed experimental compound configurations to overcome the limitations inherent in conventional helicopter designs. Recently, there has been renewed interest by the Department of Defense in the development of rotorcraft for the modern era. In 2009, the Secretary of Defense established the US Future Vertical Lift (FVL) initiative (Ref. 1) with the goal to replace all the US Department of Defense helicopters with next-generation rotorcraft in an effort to upgrade the performance and technological capabilities of the current rotorcraft fleet. One configuration that shows promise is the compound coaxial rotorcraft.

The modern compound coaxial is able to overcome limitations of the conventional helicopter by using the Advancing Blade Concept (ABC) rotor design (Ref. 2). The ABC rotor design allows each rotor of the coaxial configuration to carry a non-zero roll moment as long as the other rotor carries a roll moment of opposite direction and equal magnitude. When the rotor's roll moment is non-dimensionalized by the rotor's thrust and radius it is referred to as the lift-offset. The mathematical expression of lift-offset (L.O.) for a coaxial rotor is the following:

$$L.O. = \frac{\Delta M_x}{T_{total} R} \tag{1}$$

Presented at the Vertical Flight Society 75th Annual Forum & Technology Display, Philadelphia, Pennsylvania, May 13-16, 2019.

where ΔM_x is the differential roll moment between the two rotors, T_{total} is the combined thrust of the two rotors, and R is the rotor radius of a single rotor (assuming each rotor's radius is equal). The benefit of not constraining a rotor to operate at zero lift-offset is that the rotor is then able to operate at its optimal blade section angle of attack on the advancing side, avoid stall on the retreating side, and achieve higher forward flight speeds. In contrast, thrust production of conventional helicopters is limited because of retreating blade stall. As the rotor achieves higher forward flight speed speeds it is required to produce more thrust, and eventually the blade pitch angle on the retreating side reaches a point it can no longer generate enough lift (due to retreating blade stall) to counteract the roll moment of the advancing side of the rotor. But without the constraint of each rotor having a zero roll moment the ABC coaxial rotor design can continue to have higher lift on the advancing side of the rotor as forward speed and rotor thrust are increased.

Along with the benefits of a coaxial configuration, there are also drawbacks due to the proximity of the upper and lower rotors to each other, and operation at high speed flight. These conditions result in interference between the two rotors along with interference of the individual rotors and their own wakes. The aerodynamic interference yields impulsive loading events such as blade-vortex interaction (BVI), which results in impulsive pressure loading peaks, and therefore, impulsive noise.

Previous studies which have used theoretical modeling to predict the noise of the coaxial rotor system have focused on the variation of certain parameters to obtain overall trends. In 2005 and 2006, Boyd et al. (Ref. 3) and Wachspress (Ref. 4), respectively, published papers analyzing the noise from a coaxial rotor system. Boyd and Wachspress both noted that the coaxial rotor system on average is louder than a conventional single rotor of equivalent solidity.

One of the major studies into the noise produced by a coaxial rotorcraft utilizing lift offset was conducted at the University of Glasgow (Ref. 5) in 2009. Kim et al. used the Vorticity Transport Model developed by Brown (Ref. 6) to analyze coaxial rotor systems of varying flapwise stiffness. The paper concluded that the major source of noise was the advancing side of the lower rotor due to the interaction between the upper rotor's wake and the lower rotor's advancing side blades. And that the noise could be reduced by increasing the lift offset, especially at the higher speed case.

Walsh et al. (Ref. 7) in 2016 published an investigation into higher-speed cases of the coaxial rotor system using prescribed wake analysis. The paper noted that rotor blade phasing could potentially be used to result in noise sources adding constructively or destructively, a phenomena unique to multirotor configurations. The paper also explored the acoustic benefits of operating the rotor system at lower rotation rates, and noted significant reductions in noise levels. Also in 2016, Barbely et al. (Ref. 8) published a paper exploring the interactions between the upper and lower rotor blades at the point of crossover. Barbely et al. noted a fluctuation in pressure that is a potentially important noise source, which at that time had not been explored for its acoustic impact.

In 2018 Herrmann et al. (Ref. 9) performed a multidisciplinary trim analysis of the coaxial rotor system using a free wake model and analyzed the influence of shaft tilt on the rotor noise. Herrmann noted that at 0° shaft tilt the noise is the greatest and at +5° shaft tilt the noise appears to be the lowest. Jia et al. (Ref. 10) conducted research into higher speed cases at 0° shaft tilt using CFD analysis, and varied the lift offset and rotor separation distance. Jia noted loading fluctuations appear when the lower rotor and upper rotor blades cross one another, and the noise due to BVI events reduces as the separation distance increases at certain flight speeds.

The research efforts cited in this section all aid in the understanding of the aeroacoustic environment of the coaxial rotor system, but the complexity of the interactions makes it difficult to understand the overall implications from parametric changes without expanding the range of the parameters. The focus of this paper is on exploring a wider range of parameters and determining the influence on rotor noise. In this effort the parameters of forward flight speed, shaft angle, and lift-offset are varied and the influence on the rotorcraft aerodynamic environment and acoustics is analyzed.

ANALYSIS MODELS

This section describes the approach used to perform the analysis of the coaxial rotor configuration. Modeling of the rotor geometry, blade dynamics, trim method, airloads computation, rotor inflow, aerodynamic interference, and acoustic prediction are all summarized in the following subsections. The Rotorcraft Comprehensive Analysis System (RCAS) software (Refs. 11, 12) is used to perform the structural, aerodynamic, and trim analysis while PSU-WOPWOP (Refs. 13–15) performed the acoustic predictions.

Rotor & Trim Model

In this study a rotor system based on the Sikorsky XH-59A (Ref. 2) is modeled. The primary rotor specifications are provided in Table 1. The remaining specifications of twist, airfoil, thickness, and chord distribution of the configuration are the same as those described in the paper by Jia et al. (Ref. 10).

Table 1: XH-59A Rotor Characteristics.

Characteristic	English	Metric
Radius	18 ft	5.486 m
Number of Rotors	2	
Blades per Rotors	3	
Root Cut-Out	20%	
Blade Precone	3°	
Rotor Axial Separation	2.5 ft	0.76 m
Tip Speed	650 ft/s	198 m/s

The blade is modeled with nonlinear beam elements that have five deformation degrees of freedom. The beam elements can deform in lead-lag translation, lead-lag rotation, flap translation, flap rotation, and torsion degrees of freedom. The blade structural properties used correspond to those of the Sikorsky XH-59A rotor blade (Ref. 16). The rotor is setup to allow for feathering freedom, but is constrained in the flap and lead-lag directions. The only flap and lead-lag motion is that from the blade deformation.

The coaxial configuration is trimmed to zero roll moment, zero pitch moment, zero net force in the direction of flight, a specified differential roll moment, and lift force equal to the weight of the configuration (11,908 lbs). The trim controls are lateral cyclic pitch, longitudinal cyclic pitch, a force imposed in the direction of flight, differential lateral cyclic, and collective pitch. The imposed force is a stand-in for the force produced by an auxiliary thrust device (jet engine, rear mounted propeller, etc.). The collective, longitudinal, and lateral pitch inputs control the force in the lift direction, pitching moment of the rotor, and the roll moment of the rotor, respectively. And the differential lateral cyclic controls the differential rolling moment, and therefore the lift offset.

Aerodynamic Model

The sectional airloads are computed at every 3° azimuth along a lifting line using C81 look-up tables for lift (c_l), drag (c_d), and pitching moment (c_m), which are tabulated as functions of angle of attack (α) and Mach number (M). For each airfoil that is specified along the span of the rotor blade, there corresponds a separate C81 look-up table.

The rotor inflow model is based on the modified Maryland free wake model. The free wake is modeled with a wake resolution of 3° or 120 steps per revolution. The far wake, where the trailing vortices combine to form a single tip vortex, extends to 4 rotor revolutions. One aerodynamic interaction to note is the blade crossover, event which has been shown in other research papers utilizing CFD analysis (Refs. 10, 17). But in the current implementation of the free wake model in RCAS, this interaction is not predicted. This interaction is highly impulsive and has an impact on the noise of the rotor. The inability to account for this interaction may lead to an underprediction of noise.

By default, RCAS does not account for any interference effects from one rotor to another. So the user is required to specify the interference models for the rotors. The interference models account for the influence of the wake of one rotor on the other rotor's wake trajectory and rotor inflow via the Biot-Savart Law. For the case of the coaxial rotor configuration, the influence of the upper rotor's wake is experienced by the lower rotor and its wake, and vice-versa for the lower rotor's influence on the upper rotor.

Acoustic Model

The software PSU-WOPWOP is a physics-based acoustic prediction tool developed at Penn State University. The software can predict discrete frequency and broadband rotor noise for arbitrary maneuvering flight. The code is a numerical implementation of Farassat's Formulation 1A (Ref. 18) of the Ffowcs Williams–Hawkings (FW-H) equation (Ref. 19). Formulation 1A can be written as:

$$p'(\vec{x},t) = p'_T(\vec{x},t) + p'_L(\vec{x},t) \tag{2}$$

where the thickness noise is defined by

$$\begin{aligned} 4\pi p'_T(\vec{x},t) = &\int_{f=0} \left[\frac{\rho_0(\dot{v}_n + v_{\dot{n}})}{r|1-M_r|^2} \right]_{ret} dS + \\ &\int_{f=0} \left[\frac{\rho_0 v_n (r\dot{M}_r + c(M_r - M^2))}{r|1-M_r|^3} \right]_{ret} dS \end{aligned} \tag{3}$$

and the loading noise can be written as

$$\begin{aligned} 4\pi p'_L(\vec{x},t) = &\frac{1}{c}\int_{f=0} \left[\frac{\dot{l}_r}{r|1-M_r|^2} \right]_{ret} dS + \\ &\int_{f=0} \left[\frac{l_r - l_M}{r^2|1-M_r|^2} \right]_{ret} dS + \\ &\frac{1}{c}\int_{f=0} \left[\frac{l_r(r\dot{M}_r + c(M_r - M^2))}{r^2|1-M_r|^3} \right]_{ret} dS \end{aligned} \tag{4}$$

where p' is the acoustic pressure; $f = 0$ defines the blade surface; ρ_0 and c are the density and speed of sound in the undisturbed medium (air), respectively; $r = |\vec{x} - \vec{y}|$ is the distance between the source position $\vec{y}$ and the observer position $\vec{x}$; $v_n = \vec{v} \cdot \hat{n}$ is the velocity of the surface $f = 0$ in the direction normal itself (i.e., $\hat{n}$ is an outward unit normal vector to the surface $f = 0$); M and M_r are the Mach number and Mach number component in the radiation direction of the surface $f = 0$, respectively; and l_r is the component of loading force that the surface imposes on the fluid, in the radiation direction. For this paper only the loading noise is analyzed for the coaxial rotor system. This is done by coupling the software RCAS and PSU-WOPWOP, such that the relevant output from an RCAS output is extracted and formatted to be used as input for PSU-WOPWOP. For a detailed outline of the acoustic prediction theory, method of coupling, and noise sources the coupled system considers, refer to the paper by Sharma et al. (Ref. 20).

AERODYNAMIC ANALYSIS

In this section the aerodynamic environment of the coaxial rotor system is analyzed while varying the following parameters: 1) forward flight speed, 2) rotor shaft angle, 3) lift offset. For each variation, the wake and blade loading for each rotor is analyzed. The azimuthal derivative of the normal force determines whether a rotor is experiencing rapid changes in loading (like BVI), and the wake trajectory determines the source of BVI events.

Forward Flight Speed

In this section the coaxial rotor configuration is analyzed at forward flight speeds of 50, 100, 150, and 200 knots. For each case the shaft angle was set to 0° and the lift offset to 20%.

The loading distribution over the rotor disk highlights regions of high and low loading, but it is not as easy to see regions where the loading is varying rapidly, as occurs in a parallel BVI event. To understand if a rotor experiences BVI (or other impulsive loading events) the azimuthal derivative of loading should be plotted and analyzed. For the 150 knots case, the blade loading and the azimuthal derivative of loading are plotted with respect to the radial position and azimuth angle in Fig. 1. The first row shows that loading is concentrated on the advancing sides of the upper and lower rotors, but it is not clear whether either rotor experiences any sharp fluctuations in loading. In the second row of the figure it is clear that both rotors' advancing sides experience BVI, and potentially the rear of the rotor may be experiencing BVI-like interactions as well. In order to determine the source of the BVI events the wake is analyzed next.

The side view of the upper and lower rotors' tip-vortex trajectory is plotted in Fig. 2. The upper rotor's wake trajectory is close to the rotor plane and also intersects the rear of the lower rotor. The lower rotor's wake also travels close to the lower rotor and rises slightly above the lower rotor plane.

The wake is next considered from a top view to determine the source of each BVI event. The lower rotor in Fig. 3 operates in both rotor-to-rotor and self-BVI conditions; for example at 90° there are two BVI events. To analyze the source of the BVI events, the lower rotor blade was plotted along with the tip vortices that are in closest proximity to the blade (Fig. 3).

The upper rotor and its wake are plotted in red while the lower rotor in blue. Only two tip vortices are shown in the figure be-

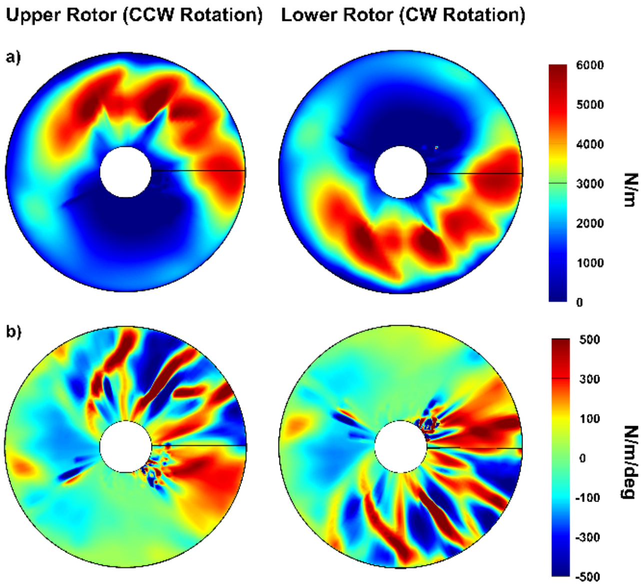

Fig. 1: Rotor normal force (row a) in units of [N/m] and azimuthal derivative of rotor normal force (row b) in units of [N/m/deg] for the upper (left column) and lower rotor (right column) with flight direction from right to left.

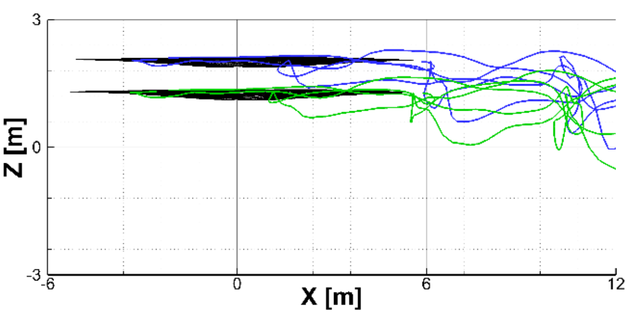

Fig. 2: Side view of the upper rotor's (blue) and lower rotor's (green) wake trajectory at 150 knots and 0° shaft tilt.

cause all other tip vortices have little to no influence on the specified BVI event. Using this same methodology the remaining BVI events on the lower and upper rotors are labeled in Fig. 4. The letters on the figure is used to specify a BVI event ("S" for self-BVI and "R" for rotor-to-rotor BVI).

The purpose of locating the source of the BVI is to understand how a change in shaft angle or lift offset will impact the BVI a rotor experiences. A forward shaft tilt results in the upper and lower rotors' wakes convecting further from the rotor. At the same time the lower rotor becomes more likely to operate in the upper rotor's wake. A change in lift offset changes the loading distribution over the rotor disk and as a result the strength of the shed wake. A change in wake strength then impacts the intensity of the BVI events. Now that the intial plots of wake trajectory and blade loading are covered, the azimuthal derivative of the normal force for all the forward flight speeds can be analyzed (Fig. 5). Each row in the figure corresponds to a different flight speed; the first column shows the upper rotor; the second column shows the lower rotor.

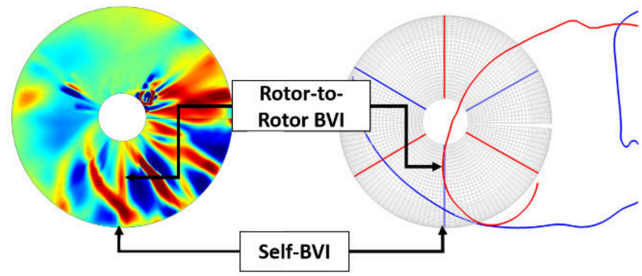

Fig. 3: Top view of azimuthal derivative of normal force for the lower rotor (left), and lower (blue) and upper (red) rotor blades and tip vortices at 150 knots (right).

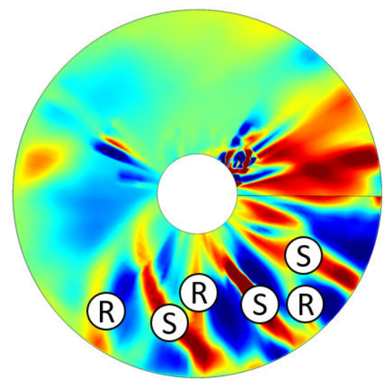

Fig. 4: Locations of BVI on the lower rotor at 150 knots, 20% lift offset, and 0° shaft tilt. "R" for rotor-to-rotor BVI event and "S" for self-BVI event.

At 50 knots the BVI events are minimal, but as the flight speed increases the BVI events increase in number and intensity. To understand how the blade are interacting with the wake, the wake trajectory is analyzed next. The trajectory of the wake for the first 3 flight conditions is plotted in Fig. 6. The first row of the figure shows the tip-vortex trajectories from the upper rotor, and the second row shows those from the lower rotor. The tip vortices for the 50, 100, and 150 knots cases are colored red, green, and blue, respectively.

As the flight speed increases the shed wake tracks closer to the rotor plane, until 150 knots where the tip vortices are approximately parallel to the rotor tip-path plane. The wake from the upper rotor convects rearward and downward (depending on the flight speed) while the wake from the lower rotor initially travels upward before following a rearward and downward trajectory, with the lower speed cases having a higher initial upward trajectory. The rotors are closely spaced to one another and this proximity may be influencing the initial trajectory of the wake. In a future exploration, the axial separation distance should be varied to determine the relationship between rotor spacing and the upward trajectory of the lower rotor's wake.

In the following sections, the rotor shaft angle and lift offset are varied for 100 knot and 150 knot cases. Before performing that analysis, it is useful to identify the source of the BVI events (which are labeled in Fig. 7). The 100 knot case expe-

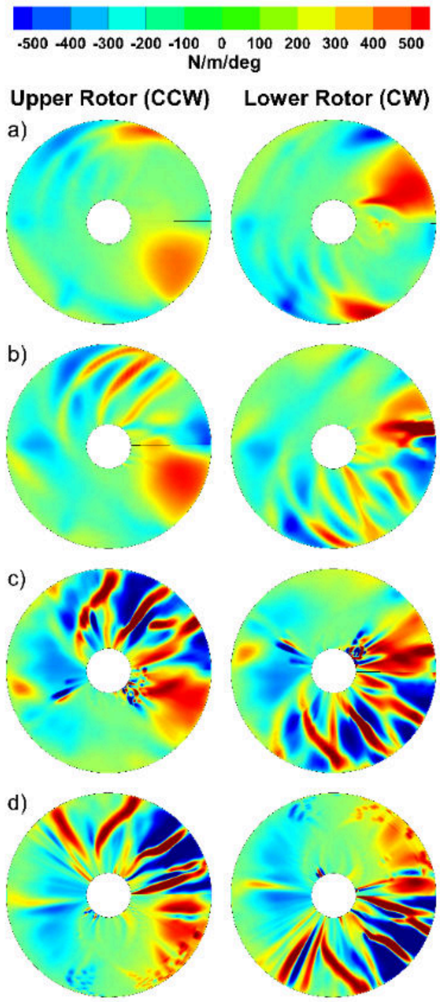

Fig. 5: Azimuthal derivative of blade loading [N/m/deg] with rotor disks moving from right to left at 0° shaft tilt and 20% lift offset. a) 50 knots b) 100 knots c) 150 knots d) 200 knots.

riences only self-BVI on the upper rotor, while the 150 knot case experiences both self-BVI and rotor-to-rotor BVI. The lower rotors for both cases also experience rotor-to-rotor BVI and self-BVI.

Rotor Shaft Angle

The next parameter to be varied is the rotor shaft angle. The shaft angle, along with the forward flight speed, is the primary factor which controls the trajectory of a rotor's wake. The increase in flight speed, as shown in the previous section, pushes the wake more rearward. The shaft angle adjusts the position of the rotor relative to the wake. For example, a forward tilt increases the relative angle between the rotor and the wake and a rearward shaft tilt reduces the relative angle. In this paper a negative shaft tilt is a forward tilt and a positive shaft tilt is a rearward tilt.

The 100 knot case is the first to be analyzed. The lift offset is set to 20% and the shaft angle is varied from +5° to -10°. The wake trajectories of the upper and lower rotors are plotted in

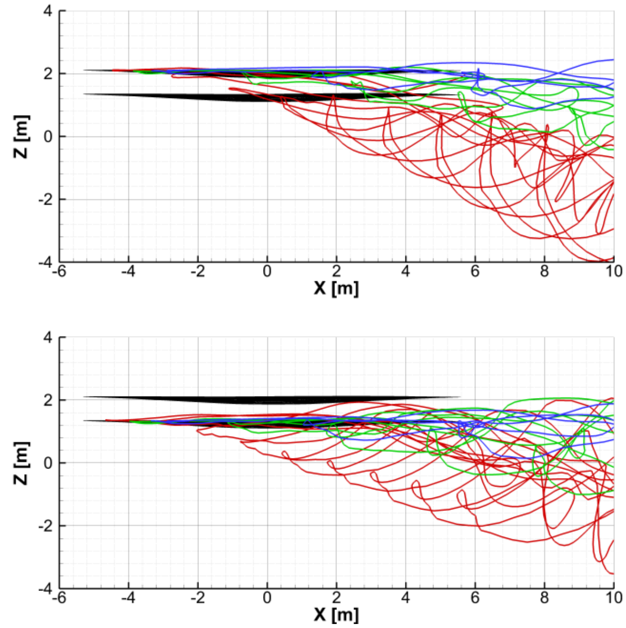

Fig. 6: Rotor tip vortices trajectory (top - upper rotor; bottom - lower rotor) at 50 knots (red), 100 knots (green), and 150 knots (blue) for 0° shaft tilt.

Fig. 8 for this comparison. The orientation of the figure is such that the rotors are plotted parallel to the x-axis, and the relative inflow to the rotor varies for the +5° and -10° shaft tilt. Consequently, the convection of the wake changes with shaft tilt as well. At +5° shaft tilt the wake is nearly parallel to the rotor plane for the upper rotor, and the lower rotor's wake moves above the rotor plane. At -10° shaft tilt both rotors' wakes move downward and rearward (relative to the rotor plane).

The azimuthal derivative of normal force for 100 knots is plotted in Fig. 9. Each row is a different shaft tilt with the first column showing the upper rotor and the second column showing the lower rotor. At +5° shaft tilt the self-BVI events (see Fig. 7) increase in intensity relative to the 0° shaft tilt. A BVI event appears around 15° azimuth on the upper rotor at +5° shaft tilt. This BVI event is due to the lower rotor's wake interacting with the upper rotor (rotor-to-rotor BVI). As the shaft tilts forward the self-BVI events on the upper rotor reduce in intensity and at -10° shaft tilt all the BVI events disappear. The lower rotor's rotor-to-rotor BVI event at 90° azimuth increases in intensity as the shaft tilts forward and all the self-BVI events subside.

The second case is the 150 knot case with 20% lift offset and a shaft angle range from 0° to -15°. The wake trajectory of the upper and lower rotor at 150 knots at 0° and -15° is plotted in Fig. 10. The wake from the lower rotor at -15° shaft tilt travels in a helical pattern without much deformation while all other wakes at both shaft angles have a greater degree of deformation. At 0° shaft tilt both the upper and lower rotors' wakes are parallel to the rotor plane and have minimal interactions with the other rotor, although the wake of the upper rotor

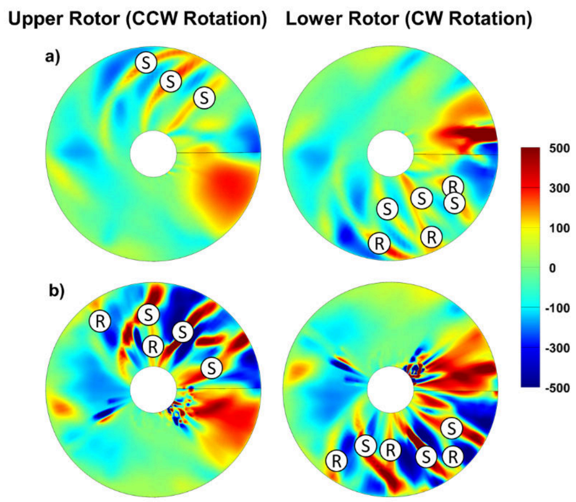

Fig. 7: Locations of BVI on the upper (left column) and lower rotor (right column) at 100 (row a) and 150 (row b) knots for 20% lift offset, and 0° shaft tilt. "R" for rotor-to-rotor BVI event and "S" for self-BVI event.

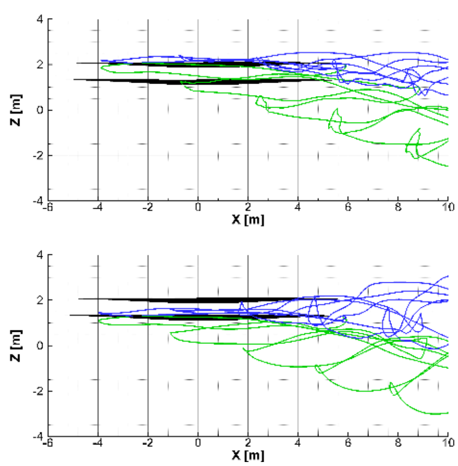

Fig. 8: Rotor wake trajectory (top - upper rotor; bottom - lower rotor) at 100 knots at +5° shaft tilt (blue) and -10° shaft tilt (green).

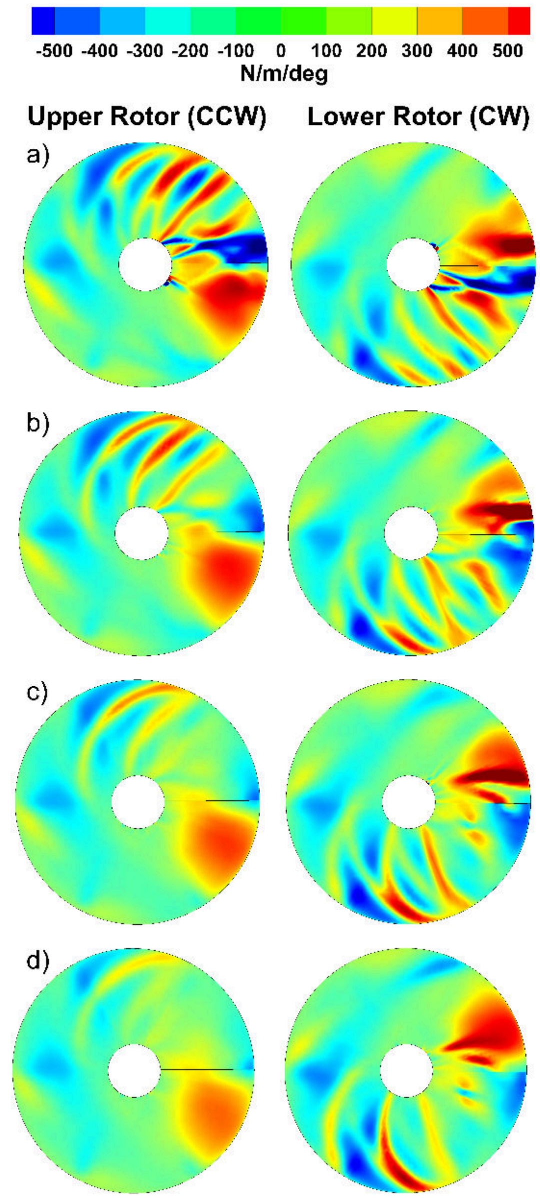

Fig. 9: Azimuthal derivative of blade loading [N/m/deg] with rotor disks moving from right to left at 100 knots. a) +5° shaft tilt b) 0° shaft tilt c) -5° shaft tilt d) -10° shaft tilt. (left column - upper rotor; right column - lower rotor)

seems to interact slightly with the rear of the lower rotor.

The plots for the azimuthal derivative of normal force are shown in Fig. 11. As the shaft tilts forward the upper rotor quickly loses the self-BVI events occurring between 0° and 90° azimuth while the self-BVI event at 90° remains. At -15° the self-BVI events on the upper rotor are no longer visible. The lower rotor's self-BVI events also reduce in intensity with the forward tilt, but a rotor-to-rotor BVI event increases in intensity and becomes the dominant source of the lower rotor's BVI (around 130° azimuth).

It should be noted that the results of Jia et al. (Ref. 17) do not show any rotor-to-rotor BVI events at a 0° shaft tilt at 150 knots. The discrepancy may be due to differences in tip vortex trajectory and strength between the CFD results of Jia and the results of free wake analysis in this paper. And these variations can have major implications on the location and intensity of the BVI events due to the proximity of the rotors. The difference between the CFD and free wake results require future study to understand the cause of the variation.

Lift Offset

Lift offset can control the lift distribution for a rotor, and because the strength of a shed vortex is dependent on the change in lift along the azimuthal and radial directions, any change to the loading along the blade will influence the strength of the shed vortex. The rotors in the coaxial configuration operated in either their own wake, in the wake of another rotor,

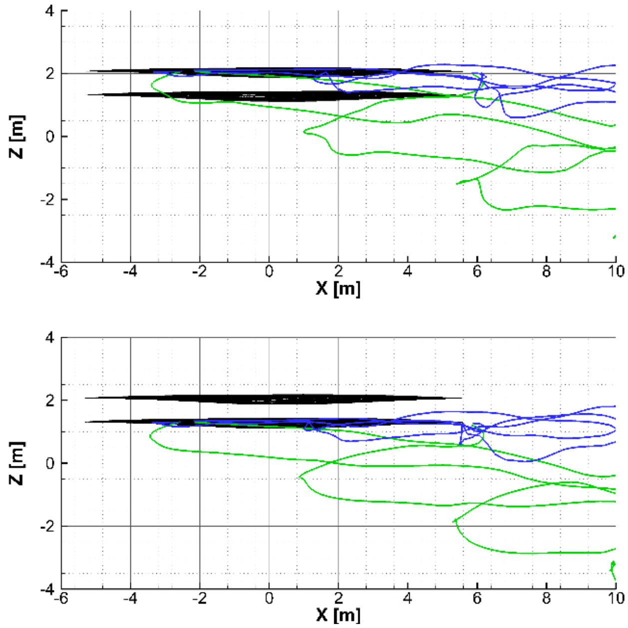

Fig. 10: Rotor wake trajectory (top - upper rotor; bottom - lower rotor) at 150 knots at 0° shaft tilt (blue) and -15° shaft tilt (green).

or a combination of both when the shaft angle was altered. When the rotor operated in its own wake the BVI events were concentrated on the advancing side. Increasing the lift offset for rotors in these conditions should also increase the intensity of the BVI events, since the wake shed on the advancing side will increase in strength. When the lower rotor operates in the wake of the upper rotor, the source of the wake is the retreating side of the upper rotor. Unlike the case of self-BVI, the intensity of the rotor-to-rotor BVI events should reduce with increasing lift offset. When the lift offset of the coaxial configuration increases, the retreating side of each rotor is offloaded, and the wake shed from the retreating side should reduce in strength. The lower rotor has rotor-to-rotor BVI events on the advancing side due to operating in the upper rotor's wake shed from the retreating side. With a reduction of wake strength from the retreating side, the rotor-to-rotor BVI events should reduce in intensity on the lower rotor.

The first case analyzed is at 100 knots and 0° shaft tilt (Fig. 12). Increasing the lift offset from 10% to 40% shows a minimal impact on the self-BVI events. The major changes are on the lower rotor with the reduction in intensity of the rotor-to-rotor BVI events and the increase of the self-BVI event around 45° azimuth. The other self-BVI events for both the upper and lower rotors show little change with an increase in lift offset.

The azimuthal derivative of loading for the case with 100 knots and -10° shaft tilt is shown in Fig. 13, which is the second case considered here. The lift offset was varied from 4% to 32% to understand the influence of lift offset on a the coaxial rotor system where the lower rotor primarily operates in the wake of the upper rotor. The upper rotor has no intense BVI conditions, so the change in lift offset has less of

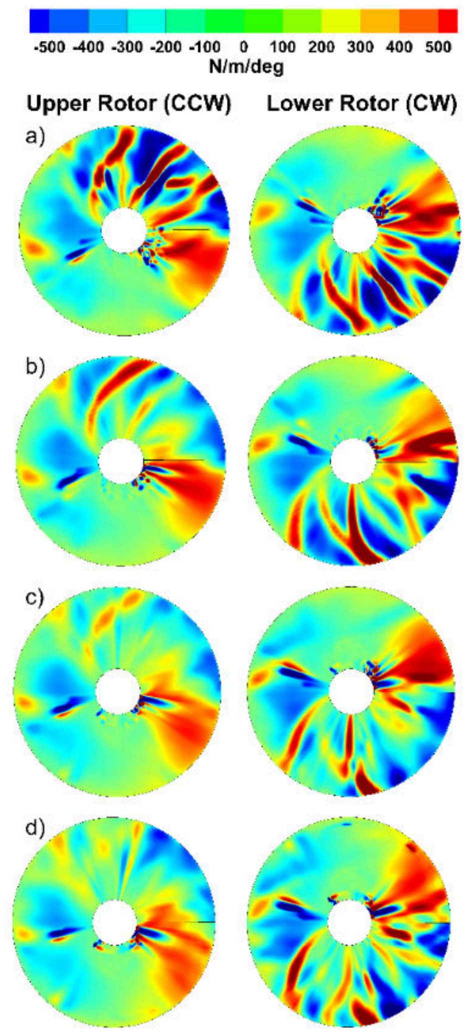

Fig. 11: Azimuthal derivative of blade loading [N/m/deg] with rotor disks moving from right to left at 150 knots. a) 0° shaft tilt b) -5° shaft tilt c) -10° shaft tilt d) -15° shaft tilt. (left column - upper rotor; right column - lower rotor)

an effect. The lower rotor at 4% lift offset has three rotor-to-rotor BVI events (highlighted in Fig. 7) that are dominant. As the lift offset increases all three events begin subsiding, but at the same time a new BVI event at the rear of the rotor begins forming around 350° on the lower rotor. This BVI event is due to rotor-to-rotor BVI from the upper rotor's advancing side. And since the wake shed from the upper rotor has the greatest strength at the greatest lift offset, the interaction with the retreating side of the lower rotor is the most intense.

The third case analyzed is at 150 knots and 0° shaft tilt (Fig 14). As the lift offset increases the only remaining BVI events are due to self-BVI. At 10% and 20% lift offset those events are not as smooth as at higher lift-offset values. Likely the reason is due to the interference from the rotor-to-rotor BVI events. But at 40% lift offset the rotor-to-rotor BVI events vanish and the three self-BVI events remain.

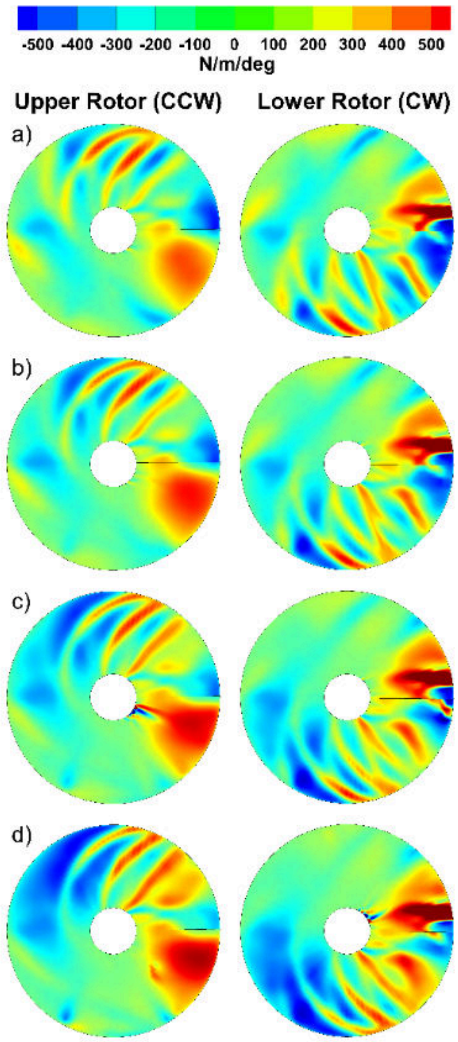

Fig. 12: Azimuthal derivative of blade loading [N/m/deg] with rotor disks moving from right to left at 100 knots and 0° shaft tilt. a) 10% lift offset b) 20% lift offset c) 30% lift offset d) 40% lift offset. (left column - upper rotor; right column - lower rotor)

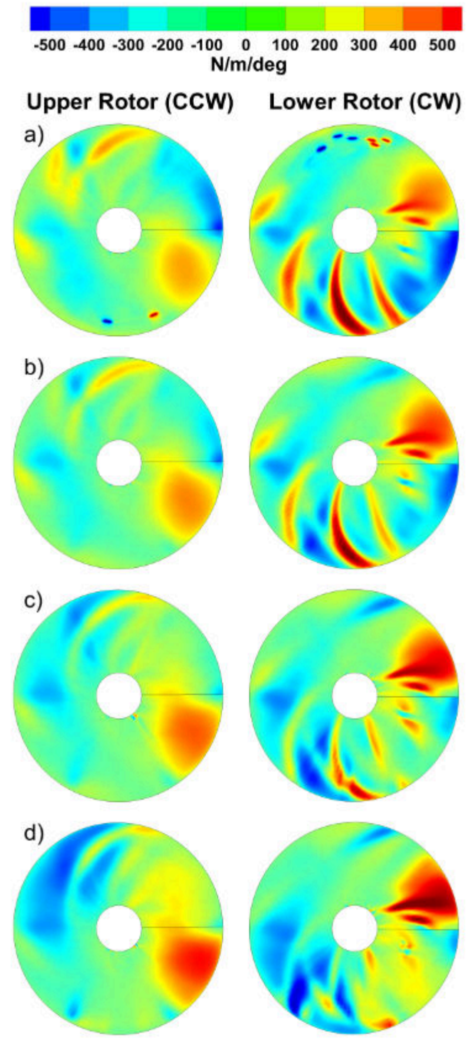

Fig. 13: Azimuthal derivative of blade loading [N/m/deg] with rotor disks moving from right to left at 100 knots and -10° shaft tilt. a) 4% lift offset b) 12% lift offset c) 24% lift offset d) 32% lift offset. (left column - upper rotor; right column - lower rotor)

ACOUSTIC ANALYSIS

In this section the parameters varied in the previously are again analyzed for their influence on rotor noise. The shaft angle and lift offset were shown to control the location of the BVI events and the intensity. These impulsive loading sources are dominant sources of loading noise as shown in Eqn. 4. The term l_r is a dominant near-field term and $\dot{l}_r$ is a dominant far field term, the loading in the radiation direction and the time derivative of loading in the radiation direction, respectively. As the magnitude and the intensity of the impulsive load sources increases, so do these terms, and therefore the noise.

The noise from the rotor system is measured on a hemisphere below the rotor that moves in the same direction and speed as the rotor. Thus the relative position of the hemisphere and the rotor system remains constant. The spherical grid has 61 points in the azimuthal direction and 31 points in the elevation direction for a total of 1891 points and each point is 10 rotor radii from the origin, which is situated at the hub of the lower rotor. The azimuth angle ranges from 0° to 360° (0° downstream from the rotor and 90° on the starboard side of the rotor) and elevation angle ranges from 0° to -90° (0° in plane of the rotor system and -90° directly below the rotor system). The hemisphere is displayed in an isometric view as well as a top view in Fig. 15 with +x-direction pointing ahead of the rotor system and +y-direction pointing to the starboard side.

The noise metric computed at each point on the grid is the mid-frequency sound pressure level (midSPL), which is an integrated noise measurement that includes the sound pressure levels in the frequency range of the 10th to 50th blade harmonic. This frequency range is typical of BVI noise. For each parametric variation the maximum midSPL and an average

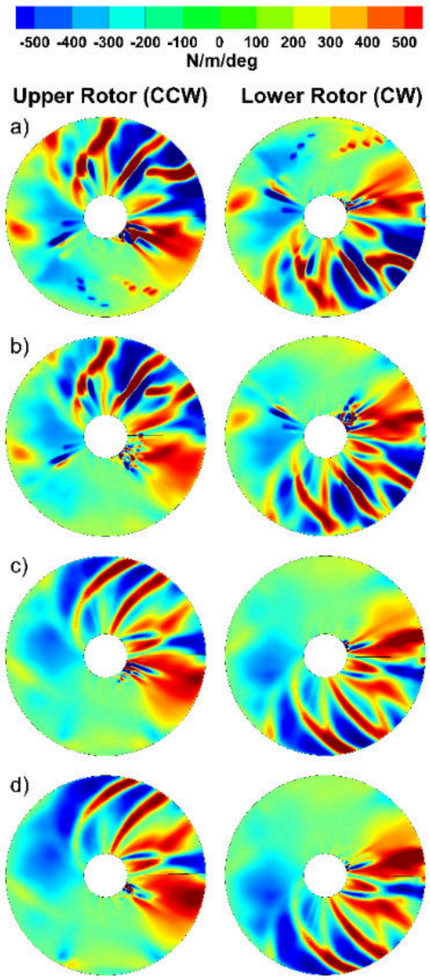

Fig. 14: Azimuthal derivative of rotor normal force [N/m/deg] with rotor disks moving from right to left at 150 knots and 0° shaft tilt. a) 10% lift offset b) 20% lift offset c) 30% lift offset d) 40% lift offset. (left column - upper rotor; right column - lower rotor)

value of midSPL over a region on the hemisphere is plotted to show the noise level and directivity. For the average midSPL measurement the hemisphere is split into 6 regions, each covering a range of 60° in the azimuth direction and -30° to -81° in the elevation direction (range of elevation shown to experience BVI). The first region ranges from 0° azimuth to 60° azimuth. In each region the average of midSPL is computed and then plotted. The hemisphere with the regions identified is plotted in Fig. 16.

Shaft Angle

The shaft angle's influence on the noise is first analyzed for 100 knots with 20% lift offset. A range of shaft angles from -10° to +5° are analyzed and the maximum midSPL is computed and plotted in Fig. 17. Each point on the graph represents the maximum midSPL on the hemispherical grid for each rotor and for the coaxial rotor system.

The noise from the lower rotor is dominant at each shaft angle. But as the shaft tilts rearward, the maximum noise levels from both rotors begin to converge. As the rotor tilts forward, the noise levels from both the rotors reduce and the difference between each rotor's maximum level increases. The largest midSPL noise levels occur at 0° shaft tilt. These results would indicate that for the 100 knots forward flight case the noise from the rotors reduce as they no longer operates in self-BVI conditions, and rotor-to-rotor BVI is preferable. The directivity, by region, of the noise is plotted for the coaxial rotor in Fig. 18.

The noise for the positive shaft tilt case is higher than the other shaft angles in all regions apart from 5 and 6, where the 0° shaft tilt case's noise is higher. The highest value of average midSPL is due to the 0° shaft tilt case, with the noise concentrated to the rear of the rotor system and the the port side. As the rotor tilts forward to -5° and -10°, the average noise levels in all regions decrease with the average noise level ahead of the rotor system being 5-10 dB lower and noise levels to the sides and rear of the rotor system are 10-15 dB lower than for the -5° and 0° cases.

The next case considered is the variation of shaft angle at 150 knots with 20% lift offset (Fig. 19). The maximum noise does not vary much with shaft angle for the coaxial rotor system. But at 0° shaft tilt the lower rotor's maximum noise level is lower than that of the upper rotor. At this shaft angle both rotors operate in self-BVI conditions. As the shaft tilts forward, the upper rotor reduces in maximum midSPL by about 10 dB, but the lower rotor remains fairly constant. At these shaft angles the lower rotor is operating in a rotor-to-rotor BVI condition while the upper rotor is operating in minimal BVI conditions. Unlike the 100 knots case, at 150 knots the rotor-to-rotor BVI for the lower rotor seems to be as important to the noise level as when it is operating in self-BVI. Whereas, for the upper rotor it is preferable to operate at a forward shaft tilt.

The average midSPL at each region on the sphere for the 150 knots with 20% lift offset case is plotted in Fig. 20. At 0° shaft tilt, the average midSPL is greatest in the front of the coaxial rotor system and lowest at the rear. As the shaft tilts forward the average noise reduces until -10° shaft tilt where the average noise begins to increase in several regions. At -15° shaft tilt, the noise is dominant in the rear. The shaft tilt determines the type of BVI interaction the rotor experiences and at a large negative tilt the lower rotor operates in the upper rotor's wake. This implies that as the noise produced by the upper rotor reduces with the forward shaft tilt as does the noise produced by the lower rotor until the rotor-to-rotor BVI noise begins to become more dominant. This trend may be true in the 100 knot case if the shaft is tilted further forward.

Lift Offset

As discussed previously in the paper, the lift offset of a rotor can control the intensity of the self-BVI and rotor-to-rotor

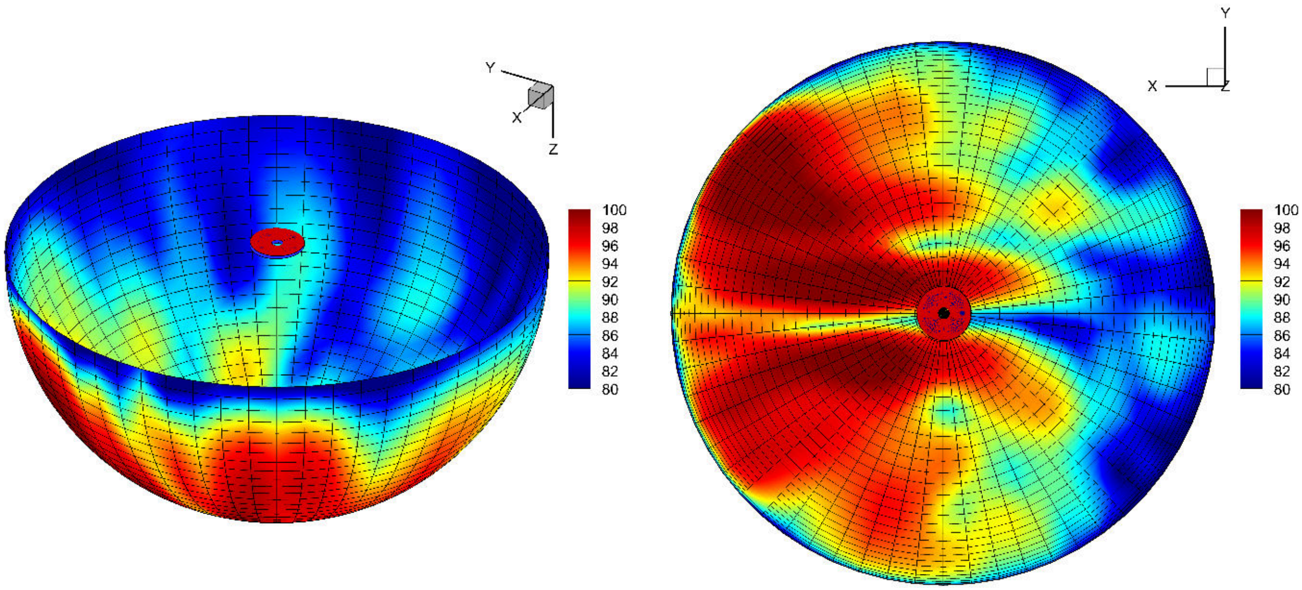

(a) Isometric view.

(b) Top view.

Fig. 15: midSPL on hemisphere with forward motion in +x-direction and starboard in +y-direction.

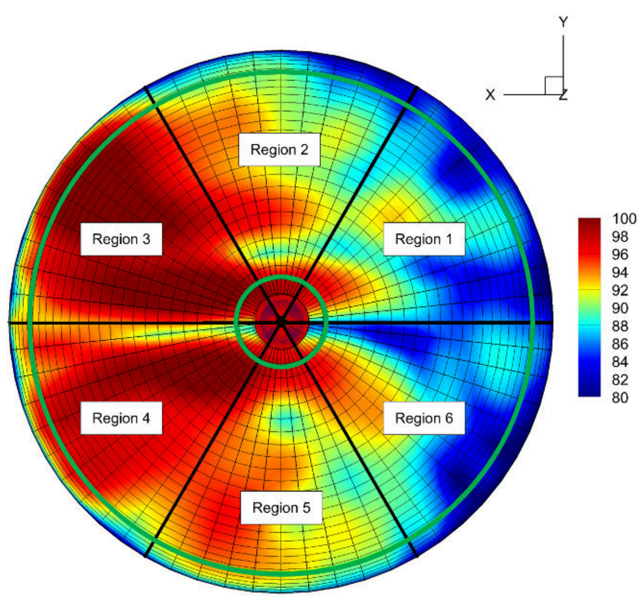

Fig. 16: Regions of the hemisphere to take the average midSPL with the elevation ranges in between the green circles and the azimuth ranges between the black lines.

BVI events. In this section the influence of lift offset on the noise produced by the rotor system is explored. Three cases are analyzed in this section: 1) 100 knots at 0° shaft tilt, 2) 100 knots at -10° shaft tilt, 3) 150 knots at 0° shaft tilt. For each case the lift offset is varied and the midSPL is computed.

The maximum midSPL for the first case (100 knots, 0° shaft tilt) is plotted in Fig. 21. For each value of lift offset the upper rotor produces less noise than the lower rotor, and the noise level remains nearly constant. The lower rotor continues to increase in maximum midSPL, but the change is minimal. The minimal change in noise is likely due to the minimal change in azimuthal derivative of normal force (Fig. 12). The directivity of the noise is shown through the average midSPL at each region (Fig. 22). The noise is concentrated towards the rear and port side of the rotor system. The noise levels also increase with lift offset. Since increasing the lift offset increases the self-BVI event intensity and reduces the rotor-to-rotor BVI event intensity, for this case the self-BVI is a more dominant noise source compared to the rotor-to-rotor BVI.

The midSPL is plotted for the second case, 100 knots and -10° shaft tilt, in Fig. 23. The lower rotor is still the dominant noise source at each value of lift offset. The maximum midSPL is lowest at 20% lift offset and increases as lift offset increases or decreases from 20%. At 20% lift offset the self-BVI events on the lower rotor begin to disappear and a BVI event on the rear of the lower rotor begins to form. At low levels of lift offset the lower rotor has multiple rotor-to-rotor BVI events and at higher values of lift offset the BVI event at the rear of the lower rotor becomes more intense. So there is a cost associated with increasing or decreasing the lift offset, and a certain value which is optimal. The average midSPL at 100 knots and -10° shaft tilt is plotted in Fig. 24. The noise levels at this shaft tilt are concentrated forward from the rotor. At low values of lift offset the maximum noise is directed towards the port side of the rotor system, and at high lift offset the maximum noise is directed towards the starboard side. The multiple self-BVI events on the retreating side are the primary source of contribution to the port side and at higher lift offset the BVI event on the retreating side of the lower rotor contributes to the starboard side. Nevertheless, the lift offset values between the two extremes have the lowest levels of noise for all regions apart from 5 and 6.

The midSPL for the final case, 150 knots and 0° shaft tilt, is plotted in Fig. 24. Unlike the 100 knot case, at 150 knots the increase of lift offset shows a favorable trend in regards to noise levels. At 10% lift offset the BVI events on both the lower and upper rotors are highly complex, and as the lift offset increases the rotor-to-rotor BVI events vanish while the self-BVI events become more intense. At the highest level of lift offset, three distinct BVI events appear on the lower and upper rotor. The directivity of the average midSPL is focused in front of the rotor system (Fig. 24). The average noise levels at 10% and 20% are similar with a difference of a few dB, and ahead of the rotor system in region 3, 20% lift offset is greater on average. But as the lift offset increases to 30% and 40%, the noise levels reduces. As stated previously, the reduction in noise can be attributed to the reduction in the total number of BVI events.

CONCLUDING REMARKS

In this paper a coaxial rotor system capable of lift offset was studied by varying the forward flight speed, shaft angle, and lift offset. The aerodynamic analysis was performed using the Maryland free wake implemented in RCAS and the acoustic prediction of the rotors' loading noise was performed by the software PSU-WOPWOP.

The aerodynamic analysis showed that the environment which the rotors operates is highly complex and there is a high probability of operating in BVI conditions. At low speeds the lower rotor operates in the wake of the upper rotor, and at higher speeds both rotors operate in their own wakes. Even when the wake is parallel to each rotor, rotor-to-rotor BVI is experienced. And at high speeds operating in minimal BVI conditions is highly unlikely, and was not possible for the cases analyzed in this paper. At low speeds the BVI contribution is minimal, but coaxial compound configurations are typically developed for the purpose of high forward flight speed.

From the aerodynamic and acoustic analysis the following conclusions have been drawn:

- Due to the proximity of the rotors, even at high speeds where the wakes convect parallel to their respective rotors, rotor-to-rotor BVI events are experienced by both the upper and lower rotors.
- At 100 knots, a forward shaft tilt can lead to noise reduction where the a reduction in self-BVI is more dramatic than an increase in rotor-to-rotor BVI. At 150 knots a forward shaft tilt initially reduces noise levels, but as the shaft tilts further forward the rotor-to-rotor BVI events become more intense as does the noise.
- When the lower rotor operates in the wake of the upper rotor it produces more noise than the upper rotor. But when the wake of each rotor convects parallel to the rotor plane both rotors begin to produce equivalent levels of noise.

This paper explored a limited matrix of parameters, and future consideration should be given to expanding the range of the parameters and including the variation of axial separation. Consideration should also be given to modeling the blade crossover interactions because, as noted by Jia et al. (Ref. 17), the forward shaft tilt increases the intensity of the crossover events. And the inclusion of the events could potentially lead to differing trends.

ACKNOWLEDGMENTS

This research was partially funded by the Government under Agreement No. W911W6-17-2-0003. The U.S. Government is authorized to reproduce and distribute reprints for

Government purposes notwithstanding any copyright notation thereon.

The views and conclusions contained in this document are those of the authors and should not be interpreted as representing the official policies, either expressed or implied, of the Aviation Development Directorate or the U.S Government.

REFERENCES

[1]Hirschberg, M., "JMR Technology Demonstration Update: The Road to Future Vertical Lift," *Vertiflite*, Vol. 62, N. 1, January/February 2016, pp. 22-27.

[2]Ruddell, A.J., "Advancing Blade Concept (ABC^{TM}) Development," 32nd Annual National Forum of the American Helicopter Society, May 1976.

[3]Boyd, D., Burley, C., and Conner, D., "Acoustic Predictions of Manned and Unmanned Rotorcraft Using the Comprehensive Analytical Rotorcraft Model for Acoustics (CARMA) Code System," American Helicopter Society International Specialists' Meeting on Unmanned Rotorcraft, Chandler, AZ, January 2005.

[4]Wachpress, D. A. and Quackenbush, T. R., "Impact of Rotor Design on Coaxial Rotor Performance, Wake Geometry, and Noise," American Helicopter Society 62nd Annual Forum, Montréal, 29 April - May 1, 2008.

[5]Kim, W. H., Brown, R.E., and Duaraisamy, K., "Effect of Rotor Stiffness and Lift Offset on the Aeroacoustics of a Coaxial Rotor in Level Flight," American Helicopter Society 65th Annual Forum, Grapevine, TX, 27-29 May 2009.

[6]Brown, R.E., Line, A.J., "Efficient High-Resolution Wake Modeling Using the Vorticity Transport Equation," *AIAA Journal*, Vol. 43, No. 7, April 2005, pp. 1434-1443.

[7]Walsh, G., Brentner, K.S., Jacobellis, and G., Gandhi, F., "An Acoustic Investigation of a Coaxial Helicopter in High-Speed Flight," American Helicopter Society 72nd Annual Forum, West Palm Beach, FL, May 17-19, 2016.

[8]Barbley, N. L., Komerath, N. M., Novak L. A., "A Study of Coaxial Rotor Performance and Flow Field Characteristics," 2016 AHS Technical Meeting on Aeromechanics Design for Vertical Lift, Fisherman's Wharf, San Francisco, CA January 20-22, 2016.

[9]Herrmann, T. A., Celi, R., and Baeder, J. D., "Multidisciplinary Trim Analysis of a Coaxial-Pusher Rotorcraft Configuration," American Helicopter Society 74th Annual Forum, Phoenix, AZ, May 14-17 2018.

[10]Jia, Z., Lee, S., Sharma., K., and Brentner, K. S., "Aeroacoustic Analysis of a Lift-Offset Coaxial Rotor Using High-Fidelity CFD-CSD Loose Coupling Simulation," American Helicopter Society 74th Annual Forum, Phoenix, AZ, May 14-17, 2018.

[11]Saberi, H., Khoshlahjeh, M., Ormiston, R. A., and Rutkowski, M. J., "Overview of RCAS and Application to Advanced Rotorcraft Problems," Proceedings of the American Helicopter Society 4th Decennial Specialists' Conference on Aeromechanics, San Francisco, CA, January 2123, 2004.

[12]Saberi, H., Hasbun, M. J., Hong, J., Yeo, H., and Ormiston, R. A., "Overview of RCAS Capabilities, Validations, and Rotorcraft Applications," Proceedings of the American Helicopter Society 71st Annual Forum, Virginia Beach, VA, May 57, 2015.

[13]Brès, G. A., Brentner, K. S., Perez, G., and Jones, H. E., "Maneuvering rotorcraft noise prediction," *Journal of Sound and Vibration,* 275(3-5):719-738, August 2004.

[14]Brès, G. A., "Modeling the noise of arbitrary maneuvering rotorcraft: Analysis and implementation of the PSU-WOPWOP noise prediction code," M.S. thesis, Department of Aerospace Engineering, The Pennsylvania State University, June 2002.

[15]Perez, G., "Investigation of the influence of maneuver on rotorcraft noise," M.S. thesis, Department of Aerospace Engineering, The Pennsylvania State University, June, 2002.

[16]Ruddell, A. J., Groth, W., McCutcheon, R., "The Advancing Blade Concept (ABC) Technology Demonstrator," United States Army Research and Technology Labratories (AVRADCOM), April 1981.

[17]Jia, Z., Lee, S., Sharma., K., and Brentner, K. S., "Effect of Pitch Attitude on the Performance and Acoustics of a Lift-Offset Coaxial Rotor Based on High-Fidelity CFD/CSD Simulations," Vertical Flight Society 75th Annual Forum & Technology Display, Philadelphia, PA, May 13-16, 2019.

[18]Farassat, F. and Succi, G. P., "The Prediction of Helicopter Discrete Frequency Noise," *Vertica,* 1983; 7(4):309-320.

[19]Ffowcs Williams, J. E. and Hawkings, D. L., "Sound Generated by Turbulence and Surfaces in Arbitrary Motion," *Philos. Trans. R. Soc. A,* 1962; 264(1151): 321-42.

[20]Sharma, K., Corle, E., Brentner, K. S., and Anusonti-Inthra, P., "Robust and Automated Coupling of RCAS and PSU-WOPWOP," Aeromechanics Design for Transformative Vertical Flight & The 5th Transformative Vertical Flight Workshop, San Francisco, CA, Jan. 16-19, 2018.

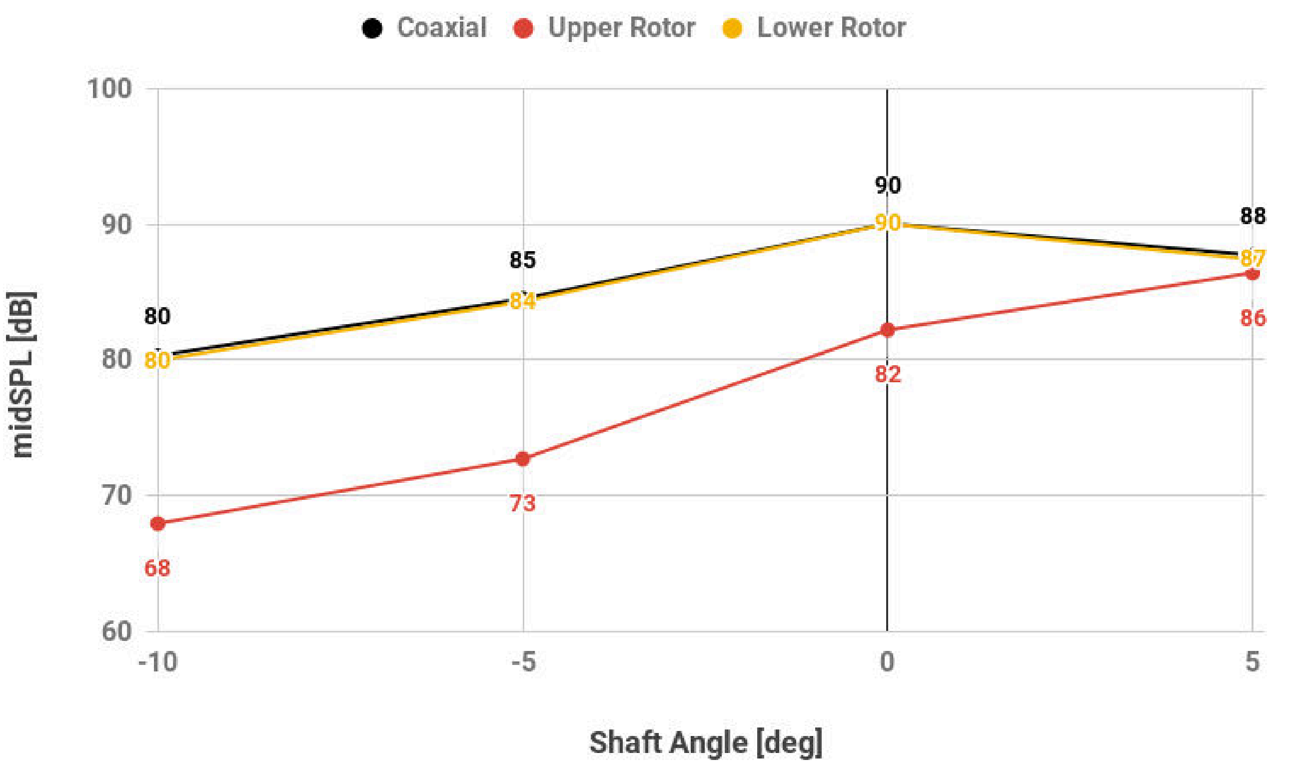

Fig. 17: Maximum midSPL values on spherical grid 10 rotor radii from rotor hub at forward flight speed of 100 knots at 20% lift offset with varying shaft angle.

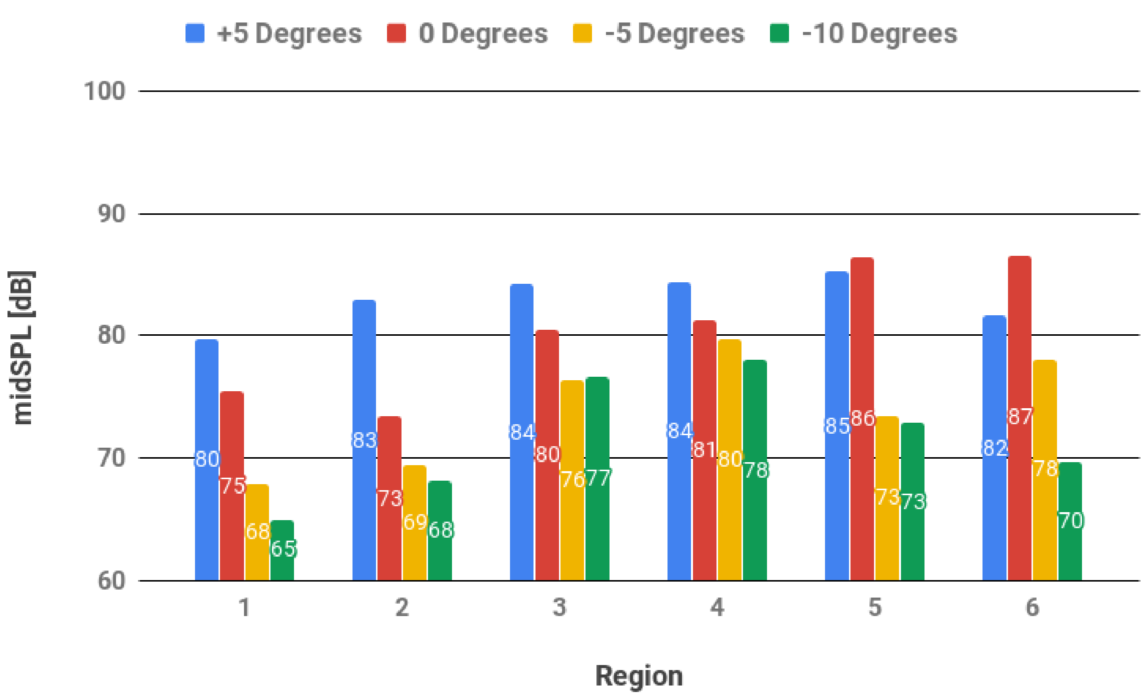

Fig. 18: Average midSPL at each region at 100 knots at 20% lift offset with varying shaft angle.

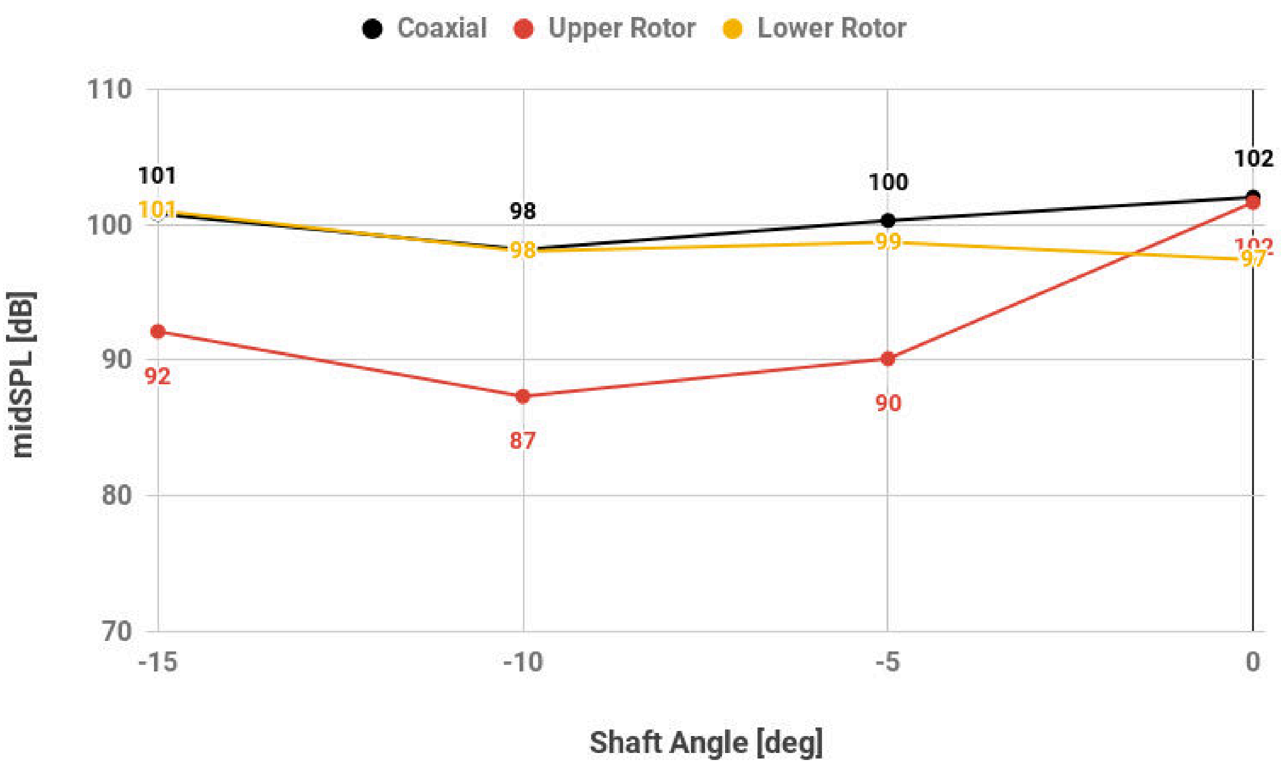

Fig. 19: Maximum midSPL values on spherical grid 10 rotor radii from rotor hub at forward flight speed of 150 knots at 20% lift offset with varying shaft angle.

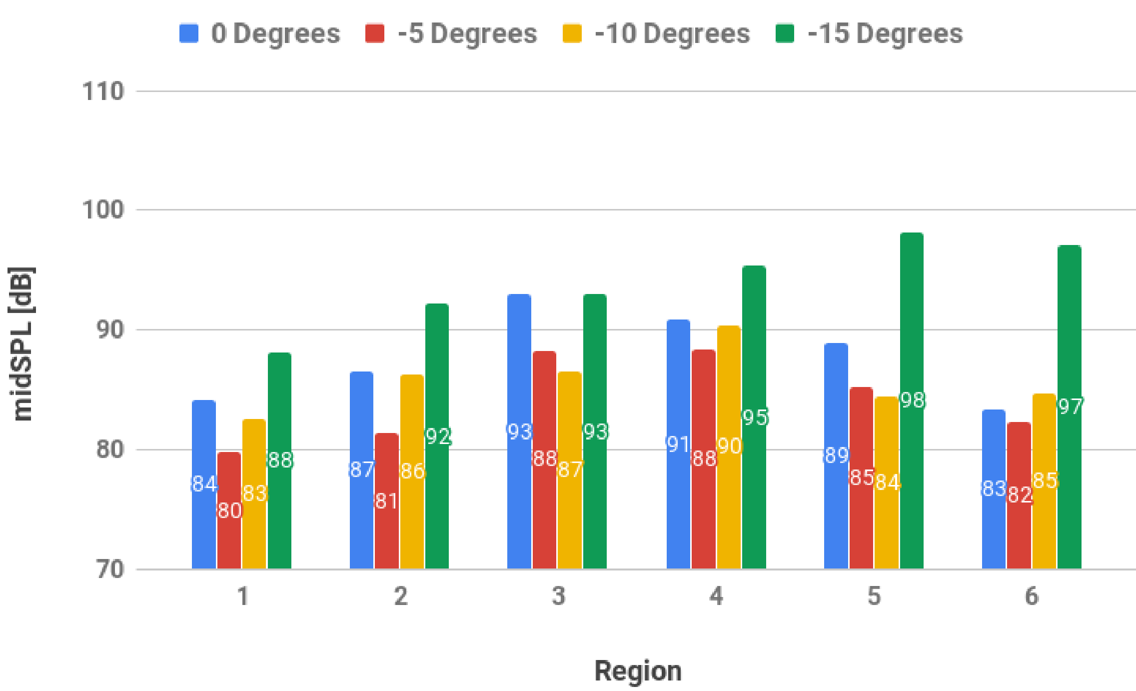

Fig. 20: Average midSPL at each region at forward flight speed of 150 knots at 20% lift offset with varying shaft angle.

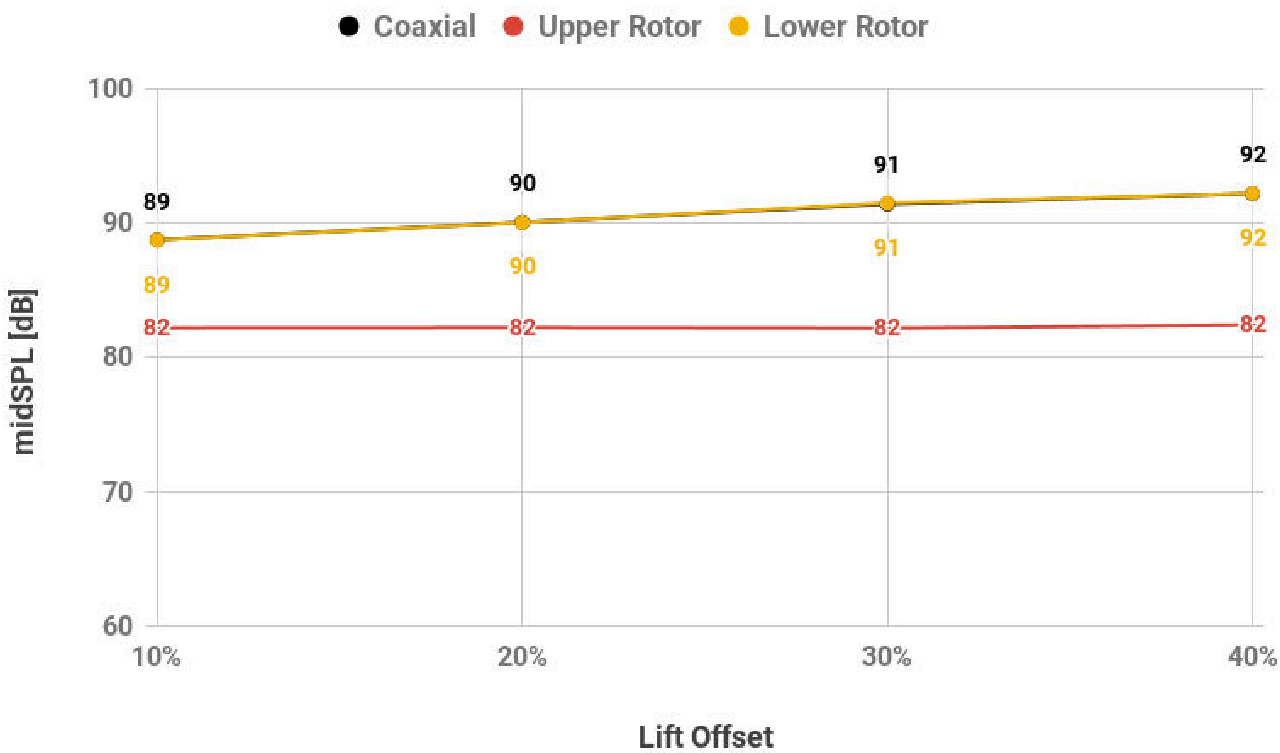

Fig. 21: Maximum midSPL values on spherical grid 10 rotor radii from rotor hub at forward flight speed of 100 knots at 0° shaft tilt with varying lift offset.

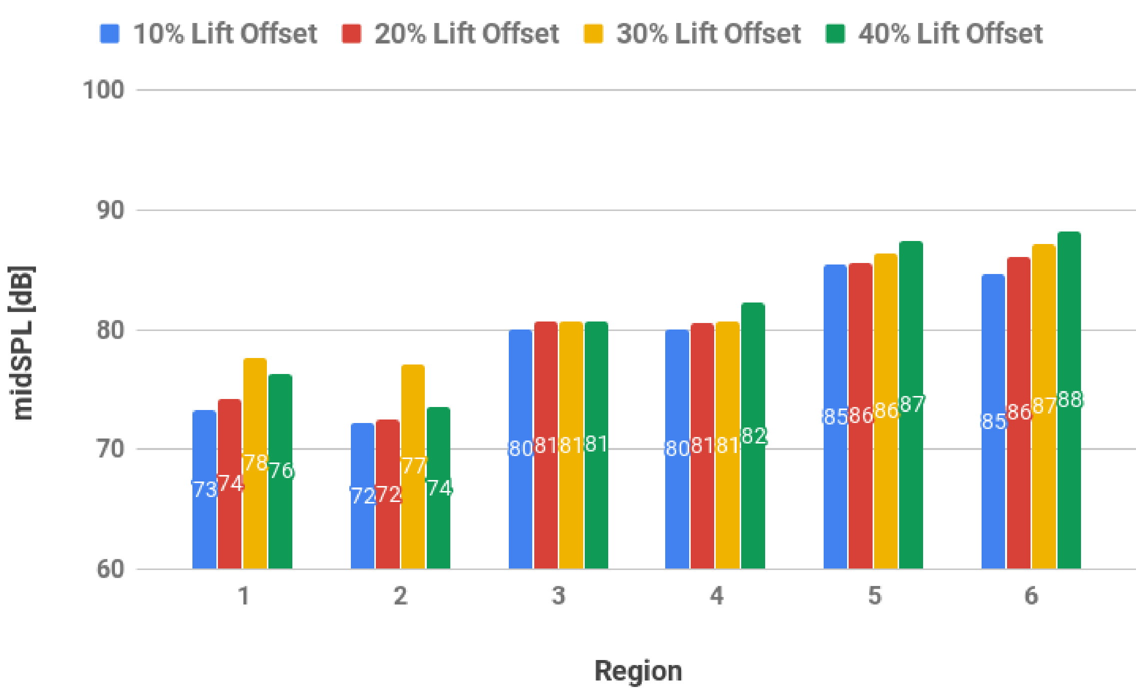

Fig. 22: Average midSPL at region at forward flight speed of 100 knots at 0° shaft tilt with varying lift offset.

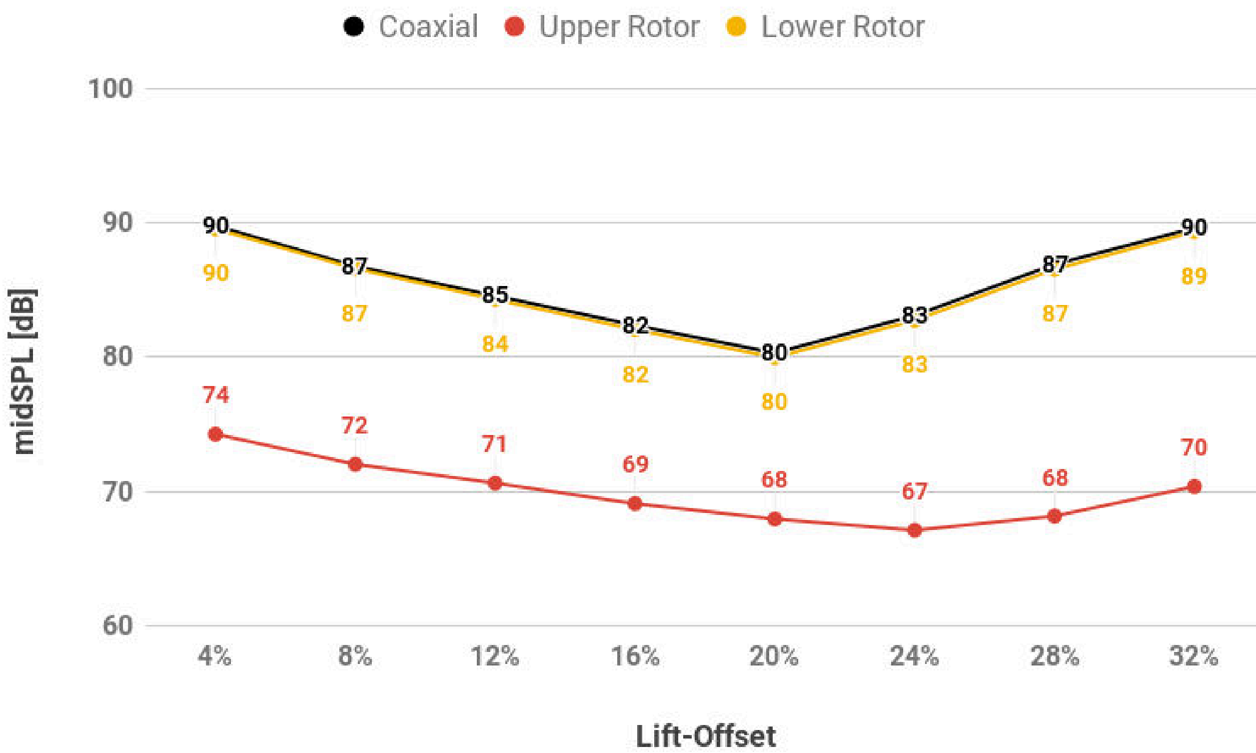

Fig. 23: Maximum midSPL values on spherical grid 10 rotor radii from rotor hub at forward flight speed of 100 knots at -10° shaft tilt with varying lift offset.

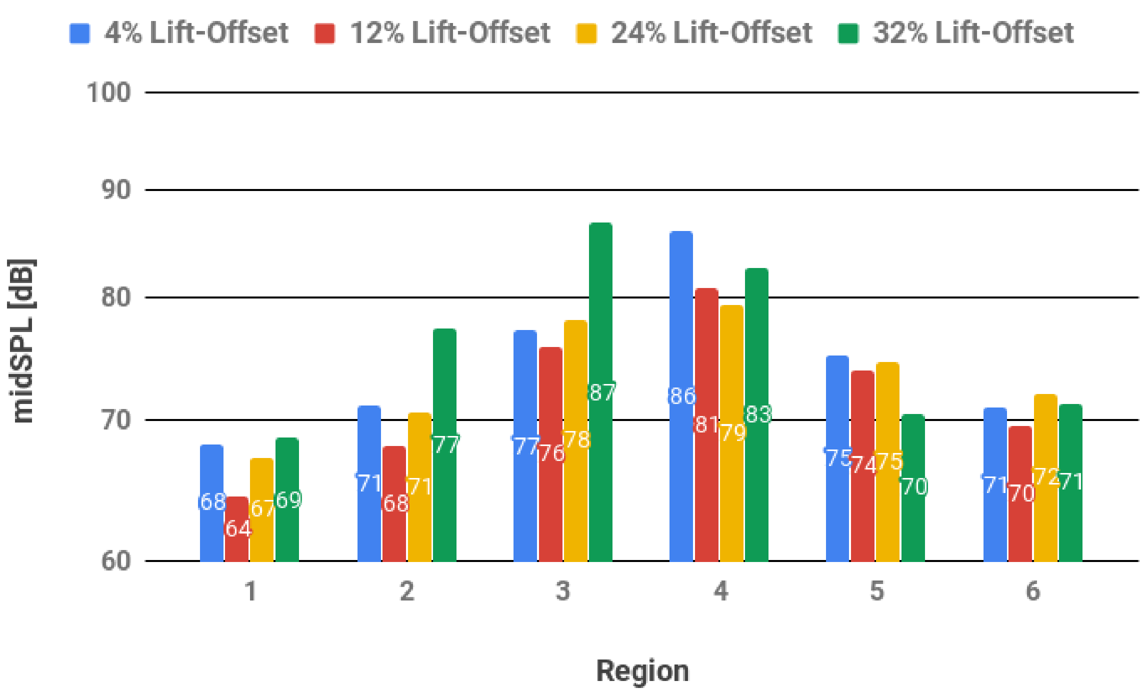

Fig. 24: Average midSPL at each region at 100 knots at -10° shaft tilt with varying lift offset.

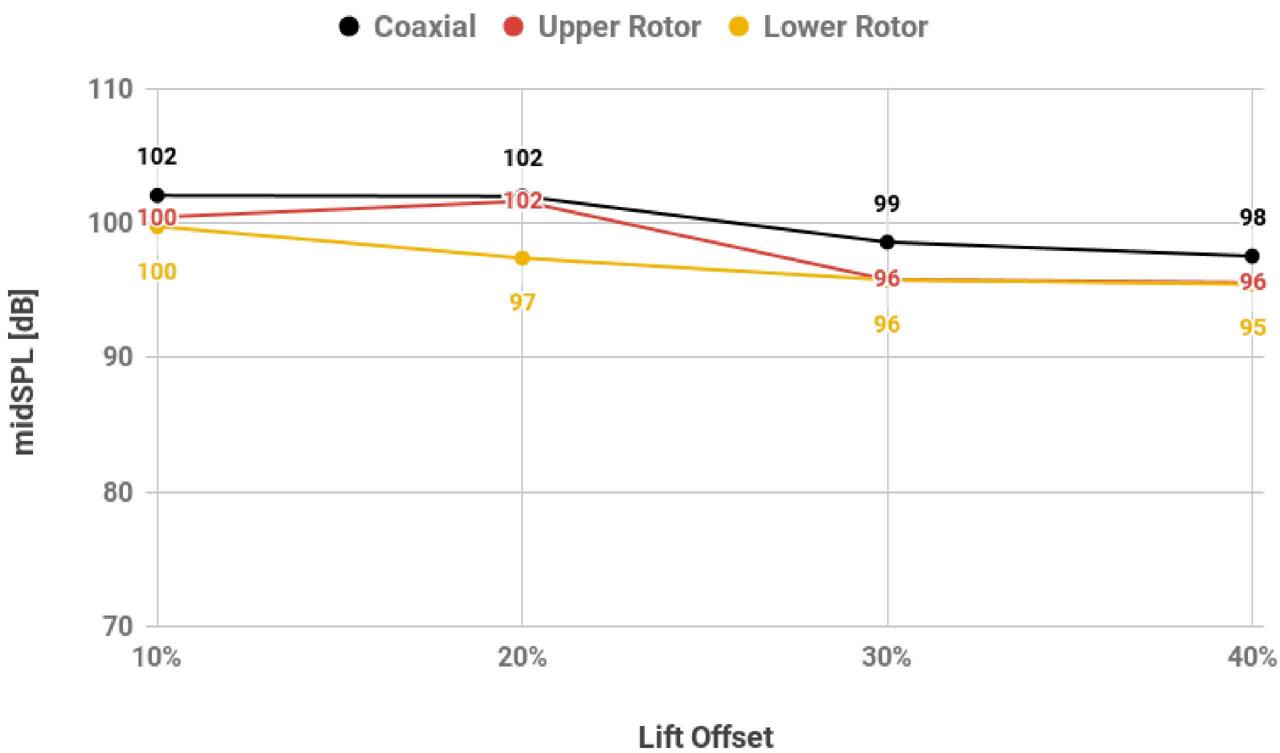

Fig. 25: Maximum midSPL values on spherical grid 10 rotor radii from rotor hub at forward flight speed of 150 knots at 0° shaft tilt and varying lift offset.

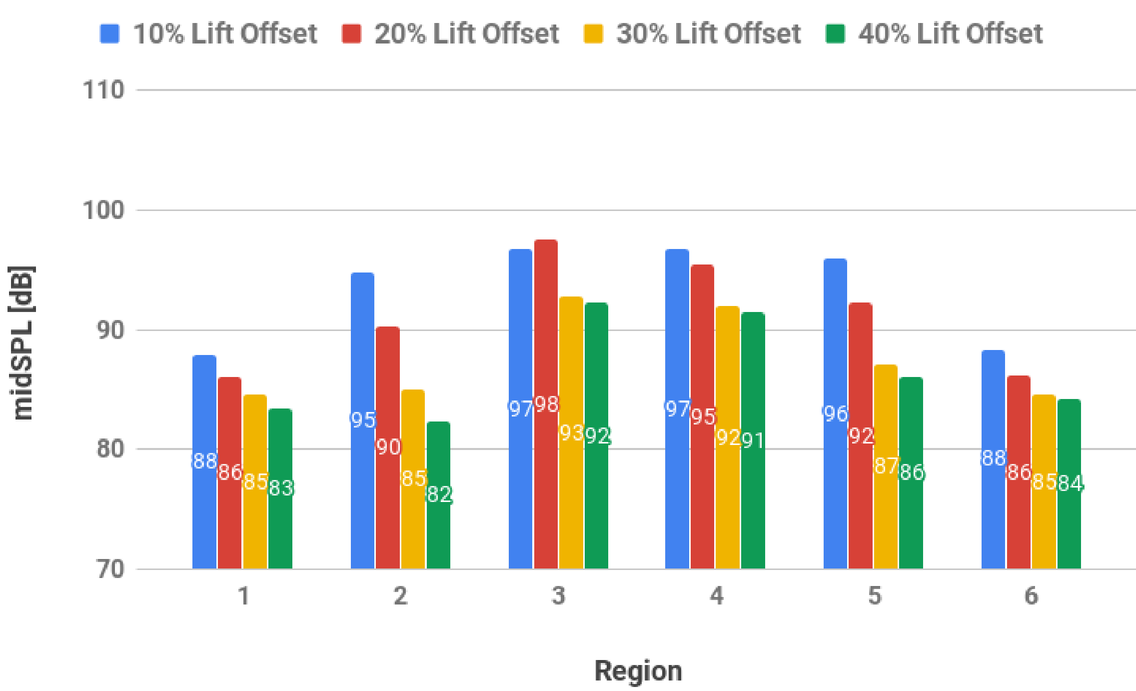

Fig. 26: Average midSPL at each region at forward flight speed of 150 knots at 0° shaft tilt and varying lift offset.